Composite Structures 312 (2023) 116856

Contents lists available at ScienceDirect

Composite Structures

journal homepage: www.elsevier.com/locate/compstruct

Influence of matrix recrystallization and nanofiller porosity on the interfacial properties of holey graphene-aluminium nanocomposites

Cátia Guarda [a], Bruno Faria [b], Nuno Silvestre [c,*], José N. Canongia Lopes [a]

[a] CQE – Centro de Química Estrutural, Department of Chemical Engineering, Instituto Superior Técnico, Universidade de Lisboa, Portugal
[b] IPC – Institute for Polymers and Composites, Polymer Engineering Department, University of Minho, Portugal
[c] IDMEC – Instituto de Engenharia Mecânica, Department of Mechanical Engineering, Instituto Superior Técnico, Universidade de Lisboa, Portugal

ARTICLE INFO

Keywords:
Interfacial shear strength
Nanocomposites
Holey graphene
Aluminium
Molecular dynamics
Recrystallization
Porosity

ABSTRACT

Due to their excellent properties, graphene-like 2D structures have been widely used to reinforce aluminium nanocomposites. However, the interfacial behaviour presented by different types of holey graphenes and their reinforcing effect on the mechanical properties of the nanocomposites are still not completely clear. In this work, Molecular Dynamics simulations are used to investigate the interfacial behaviour between five different graphenes and an aluminium matrix (Al-graphene, Al-Phagraphene, Al-haeckelite, Al-N-holey-graphene (hG) and Al-B-hG). Using pull-out loading test, the influence of the 2D nanofillers porosity on the mechanical properties of the nanocomposites is assessed. Additionally, and regarding the aluminium matrix, two different cases were studied: (i) the aluminium matrix was not recrystallized and (ii) the aluminium matrix was melted and then recrystallized. It was found that the introduction of porous graphene improves the interfacial adhesion in the nanocomposites while the pull-out force and interfacial shear strength of the nanocomposites are significantly higher when the aluminium matrix is previously melted and then recrystallized.

1. Introduction

It is well known that the performance of reinforcement nanofillers plays a key role on the mechanical properties of nanocomposites [1]. Since its discovery, graphene has been receiving significant attention due to its excellent mechanical properties, extraordinary thermal properties, and good electrical conductivity [2]. When used to reinforce aluminium (Al), graphene-like materials, have been showing a wide plethora of different conclusions regarding their effectiveness. For instance, Wang et al. [3] fabricated Al composites by adding 0.3 wt% graphene and found that the ultimate strength of the composite was enhanced by 62 %. The presence of graphene leads to a significant improvement in the strength and ductility of the composites as reported by Dixit et al. [4]. In their work, an Al-graphene composite exhibited a tensile yield stress of 94 MPa and an ultimate tensile stress of 147 MPa, much higher than 50 and 84 MPa obtained for pure Al. Shin et al. [5] fabricated Al reinforced by layered graphene and found that the tensile strength of the composite reached two times that of pure Al (up to 440 MPa) with only a 0.7 vol% graphene addition. Rashad et al. [6] investigated the mechanical properties of Al-graphene composites (0.25 wt%) and found a 13.5 % improvement in ultimate tensile strength and 50 % enhancement in failure strain over the pure Al matrix. Although great improvement in the mechanical properties of experimentally fabricated Al-graphene composites has been achieved, it is also observed that the mechanical improvement of these composites is still below the theoretical predictions [7 8], a fact that is mainly caused by insufficient interfacial bonding between graphene and Al matrix. In this type of nanocomposites, the interaction between carbon atoms of graphene and Al atoms is mainly governed by weak van der Waals (vdW) interactions [9]. Unquestionably, understanding the interfacial behaviour between graphene and Al matrix is of great significance to produce high-quality graphene-reinforced Al nanocomposites. Improving the interfacial interaction between graphene and Al matrix is presently a research focus since a good load distribution between nanofiller and matrix is determinant to increase the reinforcement of the nanocomposite. Regarding this topic, the following remarks are due:

- Chemical modification of the graphene's surface can increase the roughness of graphene and, consequently, increase the contact area with the metal matrix. Liu et al. [9] presented a strategy where the Al substrate is modified with Al_2O_3 (with or without covalent bonds formed between Al_2O_3 and graphene) or Al_4C_3 to achieve

* Corresponding author.
E-mail address: nsilvestre@tecnico.ulisboa.pt (N. Silvestre).

https://doi.org/10.1016/j.compstruct.2023.116856
Received 13 August 2022; Received in revised form 10 February 2023; Accepted 21 February 2023
Available online 25 February 2023
0263-8223/© 2023 The Authors. Published by Elsevier Ltd. This is an open access article under the CC BY-NC-ND license (http://creativecommons.org/licenses/by-nc-nd/4.0/).

Table 1
Young's modulus (Y) and yield stress (σ) in GPa, as well as yield strain (ε) are presented for pure Al and nanocomposites. The percentual variation of the mechanical properties of nanocomposites and pure Al is also given.

Structure	Y (GPa) recrystalized Al	%	σ	%	ε	%
Pure Al	76	–	5.41	–	0.074	–
Al-graphene	95	+27	7.12	+32	0.081	+10
Al-phagraphene	86	+15	6.54	+21	0.086	+16
Al-haeckelite	87	+16	6.40	+18	0.076	+4
Al-N-hG	75	0	4.08	−25	0.061	−17
Al-B-hG	78	+4	6.37	+18	0.083	+13

substantially improved interfacial shear strength and overall mechanical properties of Al-graphene composites. The results showed that this strategy works very well and among the three cases considered, modifying Al substrate by Al_2O_3 without covalent bonds formed at the interface between Al_2O_3 and graphene produces the strongest interfacial interaction and excellent mechanical properties. However, in the presence of covalent bonds, the reinforcing effect is adversely affected due to the sp^2–sp^3 bond transformation which partially degrades graphene.

- Metals, such as Ni, Cu, Ti and Pt, can strongly bond with pristine graphene due to coupling between their d-orbitals and carbon atoms of graphene [10 11]. Thus, coating metal species on graphene can promote the interface adhesion between Al matrix and graphene. Wang et al. [11] confirmed that coating graphene with Ni (25–100 %), can increase the interfacial bonding up to 145.34 % (depending on the percentage of coating).
- Foreign atoms, such as O, B, N and F, promote electron exchange between the carbon and metal matrix atoms to form strong covalent bonds that act as a 'bridge' between the matrix and graphene [12].
- Defects in graphene enhance the mechanical properties of Al-graphene composites considerably. Zhang et al. [13] investigated how the Stone–Wales (SW) defect, the single vacancy (SV), and the double vacancy (DV) (three typical point defects) affect the mechanical properties of Al-graphene composites. The point defects significantly increased the interfacial bonding energy and the buckling while decreasing the equilibrium interlayer distance and the minimum interatomic distance, especially SV. The interfacial bonding energy of graphene containing SV was approximately four times that of the pristine graphene.
- The barrier effect of the interface has an important role in the interaction between graphene and Al matrix. During the cooling process of Al-graphene composites, uneven interfaces between graphene and the Al matrix are produced, which can limit the deformation of Al matrix and affect the properties of Al-graphene composites. Zhou et al. [14] found that the introduction of a graphene interface could affect the formation of twisted grain boundaries during the crystallization process. The excellent load-bearing capacity of graphene interface plays an important role in the reinforcement of Al- graphene composites.

Although several studies have been focusing on the mechanical properties of Al-graphene nanocomposites, little is known regarding the reinforcement effect of adding holey type graphene nanofillers to Al nanocomposites. Laboratory testing at the nanoscale is usually expensive, sensitive to a wide range of factors that may influence the experiment itself, technically complex and time consuming. An excellent alternative has been Molecular Dynamics (MD) simulations, which are one of the most powerful theoretical tools for nanoscale analysis [7 15], due to their good accuracy and potential to study nanoscale phenomena with great detail. In a previous work [16], the authors used MD to investigate (i) the effect of the nanofillers porosity in Al recrystallization, (ii) the orientation of recrystallized Al atoms at the interface and (iii) the mechanical properties of these nanocomposites under tensile loading. The main results of that work, in terms of improvement of the mechanical reinforcement of the nanocomposites by the introduction of nanofillers are presented in Table 1.

The main objective of this work is to use MD to assess the causes of the reinforcement effect of adding holey-type graphene nanofillers to Al nanocomposites and to evaluate the adhesion between the latter and Al at the interface. The interfacial behaviour of five nanocomposites (Al-graphene, Al-Phagraphene, Al-haeckelite, Al-N-holey-graphene (hG) and Al-B-hG) is analysed using pull-out loading test. The effect of nanofiller porosity and aluminium matrix melting and recrystallization

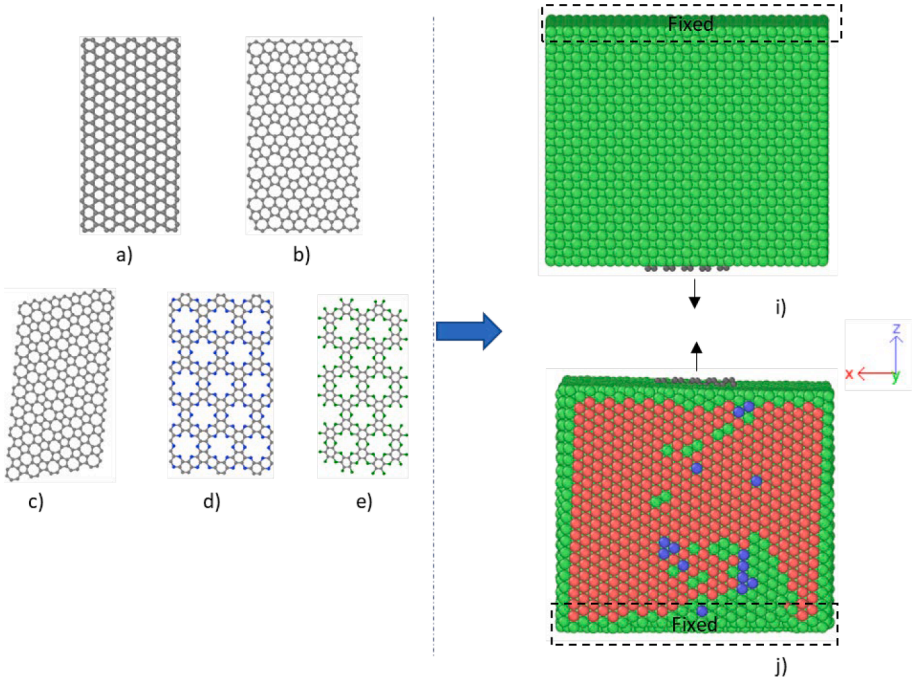

Fig. 1. Atomic configurations. a) Gr; b) Phagraphene; c) Haeckelite; d) Al-N-hG; e) Al-B-hG; i) front view of Al-graphene nanocomposites without melted and recrystallization; j) perspective view of Al-graphene nanocomposites after recrystallization. Grey, blue, green, and pink colours denote carbon, nitrogen, boron and Al atoms. In Figures j) and i), the green colour shows FCC atoms, the red colour shows HCP atoms and the blue colour BCC atoms. (For interpretation of the references to colour in this figure legend, the reader is referred to the web version of this article.)

Table 2
Structural data on nanocomposites. **H** is depth (defined in the y-direction of the crystal lattice); **W** is width (defined in the x-direction of the crystal lattice); **L** is length (defined in the z-direction of the crystal lattice); **N** is the total number of atoms; and **Fc** is the carbon volume fraction.

		a (Å)	H (Å)	W (Å)	L (Å)	N	F_c (%)
Matrix	Al	4.041	64.8	64.8	81.0	22,325	
Sheet	Graphene			19.9	39.4	330	
	Phagraphene			21.7	40.5	376	
	Haeckelite			22.2	40.4	359	
	N-hG			24.1	41.8	318	
	B-hG			22.5	46.9	286	
Nanocomposite	Al-graphene		64.8	64.8	81.0	22,246	1.5
	Al-phagraphene					22,252	1.7
	Al-haeckelite					22,235	1.6
	Al-N-hG					22,126	1.4
	Al-B-hG					22,048	1.3

is assessed by comparing two different cases. The potential energy and pull-out force are extracted and plotted as a function of displacement. From pull-out force, the maximum pull-out force and interfacial shear strength are computed and presented as a function of carbon atoms density in the sheets. Finally, the interaction energies for case A and case B are presented and their variations are discussed as a function of the structural differences between the interfaces in both cases.

2. Computational approach

2.1. MD models and potentials

The Al matrix was modelled according to lattice constant in the form of a square prism (see Fig. 1). The nanofillers were also modeled, with a thickness of 3.35 Å. Pristine graphene was modelled from the in-built extension "Nanotube Builder" in the software Visual Molecular Dynamics (VMD) [17,18]. From the configuration obtained in VMD for the pristine graphene sheet, it was possible to model N-hG and B-hG using manual editing in the software Avogadro [19]. R-haeckelite and phagraphene sheets were modelled using the software Visualisation for Electronic Structural Analysis (VESTA) [20]. The dimensions, number of atoms, and carbon volume fraction of the nanocomposites can be seen in Table 2.

To obtain the initial configuration of the nanocomposites, a set of Al atoms was removed from the central region of the prism and a vacant layer with dimensions equal to those of the nanofillers was left. The nanofillers were then inserted into the respective Al prisms, ensuring a minimum distance of 2 Å between the nanofiller atoms and the Al atoms along the nanocomposite interface, to avoid repulsive interactions at the beginning of the simulation. To facilitate the imposition of pull-out displacements, the Al matrix has been cut (along the *xy* plane at a specific z coordinate), to leave the first layer of atoms of the nanofiller visible (see Fig. 1(i)-(j)). Fig. 1(a)-(e) illustrate the different nanofillers incorporated into the Al matrix. Large-scale Atomic/Molecular Massively Parallel Simulator (LAMMPS) code [21] was adopted to perform the pull-out process of nanofillers from Al matrix. The visualization/analysis was done with the aid of Open Visualization tool OVITO [22]. The interatomic interactions between C-C, C-N, and C-B atoms were modelled with the Tersoff potential [23 24] and the interactions between Al-Al atoms were described using the embedded atom model (EAM) potential [25]. No Al-C, Al-N and Al-B bonds were introduced to model the Al-nanofillers interface (only vdW forces describe this interaction). The Lennard-Jones (LJ) 12–6 interaction potential was utilized to take care of the non-bonded interactions between Al matrix and nanofillers.

The LJ parameters for the interactions between nanofiller atoms (C, N and B) and Al atoms were calculated by the following Lorentz-Bertholet mixing rule [26]:

$$\varepsilon_{a-b} = \sqrt{\varepsilon_{a-a}\varepsilon_{b-b}} \tag{1}$$

Table 3
LJ parameters for C-C, N-N, B-B, Al-Al and C-Al, N-Al and B-Al non-bonded interactions.

Non-bonded interaction	ε_{a-b}(eV)	σ_{a-b}(Å)
C-C [27]	0.00296	3.407
N-N [28]	0.00910	4.289
B-B [29]	0.00412	3.453
Al-Al [30]	0.41570	2.620
C-Al	0.03508	3.014
N-Al	0.06167	3.455
B-Al	0.04136	3.037

$$\sigma_{a-b} = \frac{1}{2}(\sigma_{a-a} + \sigma_{b-b}) \tag{2}$$

where ε and σ are the coefficient of well-depth energy and the vdW equilibrium distance of null potential, respectively. The value of ε_{a-b} was obtained from Eq. (1) between ε_{a-a} (C, N or B) and ε_{b-b} (Al) and the value of σ_{a-b} was obtained from Eq. (2) between σ_{a-a} (C, N or B) and σ_{b-b} (Al). Table 3 summarizes the LJ parameters for C–C, N-N, B-B and Al-Al non-bonded interactions [32 33 34 35] and the calculated parameters for C-Al, N-Al and B-Al non-bonded interactions. A cut-off distance of 10.0 Å was chosen.

2.2. Holey graphene porosity

Pristine graphene is composed of 6-C rings, which serve as building blocks for sp^2-bonded low-dimensional carbon structures. When two π-bonded C atoms in pristine graphene are rotated by 90° it forms two 5-C rings and two 7-C rings, resulting in structures such as R-haeckelite [13]. In phagraphene, 5- and 7-C rings pairs are surrounded by 6-C rings. These pairs are arranged in a rectangular shape [31]. A hollow pore is formed by intentionally removing a large number of C atoms from the graphitic plane to produce holes distributed on the atomic thickness of the graphene sheet [32].

The equilibrium distances of the "pores" and corresponding interior areas were calculated (see Table 4) without considering atomic VdW radius. Porosity is normally defined has the volume of void space in pores divided by the overall volume. In this case, the only truly void or hollow space are in biggest pores in the Al-N-hG and Al-B-hG structures since 6-C rings and 7-C rings are not considered permeable. Therefore only Al-N-hG and Al-B-hG structures have porosity. With the objective of having a common ground to compare the nanofillers "pore" irregularities, this work uses the equilibrium distances of the bigger pores present in the structures and also the atomic density defined as the number of carbon atoms per unit area of sheet.

Table 4
Equilibrium distances (d) and areas (A) of 5-C ring (5′C-C); 6-C ring (6′C-C); 7-C ring (7′C-C); 6-N or 6-B ring (6′C-X); and hollow sites (hollow) of nanocomposites, in Å.

Structure	5′C-C		6′C-C		7′C-C		6′C-X		Hollow	
	d (Å)	A (Å^2)	d (Å)	A (Å^2)	d (Å)	A (Å^2)	d (Å)	A (Å^2)	d (Å)	A (Å^2)
			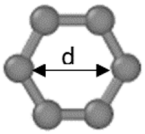		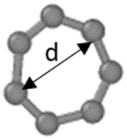		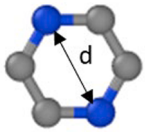		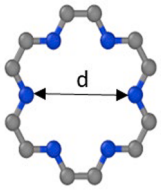	
Al-graphene			2.85	5.46						
Al-phagraphene	2.25	3.28	2.85	5.46	3.26	7.53				
Al-haeckelite	2.25	3.28			3.26	7.53				
Al-N-hG			2.85	5.46			2.84	5.24	5.67	20.96
Al-B-hG			2.85	5.46			2.98	6.65	6.07	24.49

2.3. MD simulation procedure

Initially, the simulation system was equilibrated using the NVT[1] ensemble and Nosé-Hoover thermostat for 100 ps at 10 K temperature. The Velocity-Verlet algorithm was employed to update the position and velocity of the atoms of simulation system. A time step of 1 fs was adopted. Periodic boundary conditions were applied to the × and y directions while the free boundary condition was imposed to the loading direction (z-direction). After the equilibration, the nanofillers' atoms were forced to move by using a displacement-controlled method. The first layer of visible atoms of the nanofiller was subjected to constant displacement along the z-direction at a velocity of 0.04 Å/ps until the nanofiller was completely pulled out from Al matrix. The three atomic layers on the opposite side of the Al matrix where displacement were imposed were fixed during the pull-out procedure.

In order to understand the influence of recrystallization on the interfacial behaviour, the procedure described before was applied to two different cases: (i) case A, in which the Al matrix was not modified (neither melted nor recrystallized), and (ii) case B, in which the Al matrix was melted and then recrystallized. Note that case B resembles a more realistic approach since it involves melting the Al matrix, thus allowing a closer grasp of the effect of the porosity of the nanofillers on the interfacial adhesion of the nanocomposites. However, the case B requires a significant increase in the simulation workload since it involves a melting step and then a recrystallization step. By determining the extent to which this step captures the effect of the porosity of the nanofillers, the results of the simulations that will be shown in this paper will provide an informed decision on whether to employ the recrystallization of aluminium matrix.

The method described above and these same nanofillers were previously utilized to i) determine the effects of defective structures in graphene on the recrystallization yield of Al, as well as to ii) calculate the mechanical properties of these nanocomposites under tensile loading. The results were published in reference [16]. The present paper describes the results of a complementary work to presented in [16], but focused on the adhesion behaviour between the metal-graphene type nanofiller.

3. Results and discussion

3.1. Case A – bare aluminium matrix

To characterize the interfacial performance of Al-nanofillers, the potential energy and pull-out force of the simulation system were

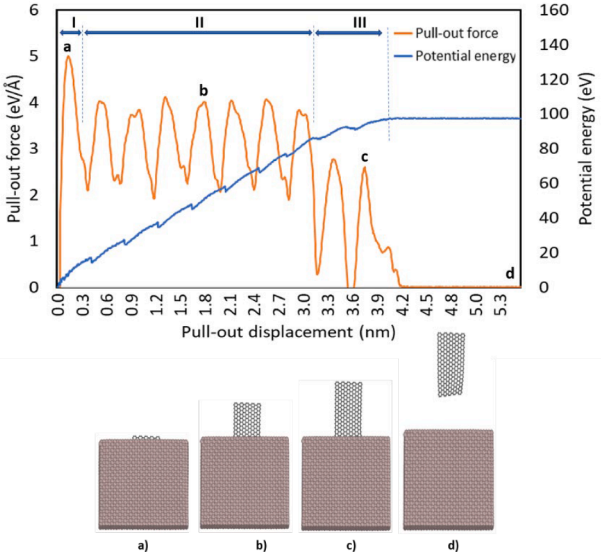

Fig. 2. Pull-out force and potential energy variation as a function of pull-out displacement for Al-graphene nanocomposite (case A). The snapshots show the atomic configurations at different pull-out displacements.

obtained from MD simulations. Fig. 2 presents the variation of the potential energy and pull-out force with the pull-out displacement in case A for the graphene sheet. The snapshots in Fig. 2 represent the atomic configurations during the evolution of pull-out procedure. It can be observed that the pull-out force (orange line) can be divided into three stages, i.e. stage I, II and III. In the first stage (I), the force rapidly increases and rapidly reaches a maximum value. In the second stage (II), the pull-out force fluctuates around a mean value (3.2 eV/Å) – here we call it the stationary stage because the force values oscillates about a mean value. This value is in close agreement with the results published by Zhu et al. [15] for Al-graphene nanocomposite [1 1 0] and by Wang et al. [11] for uncoated graphene/Al composite. In the third stage (III), the pull-out force drops with the detachment of graphene from Al. The pull-out force drops to zero (see Fig. 2(d)) and interaction ceases between the two materials. It can also be observed that the potential energy (blue line) of the simulation system increases gradually, with very small oscillations, during the pull-out test and reaches a maximum, being constant after that (horizontal plateau).

Fig. 3 is similar to Fig. 2 (Al-graphene nanocomposite) but applies to holey graphene Al nanocomposites (Al-phagraphene, Al-haeckelite, Al-N-hG and Al-B-hG). The variation of pull-out force (orange line) can also be divided into the same three distinct phases. Initially, the force increases as well and reaches a maximum value in stage I within the range

[1] In the NVT ensemble the number of molecules (N), volume (V), and temperature (T) are kept constant.

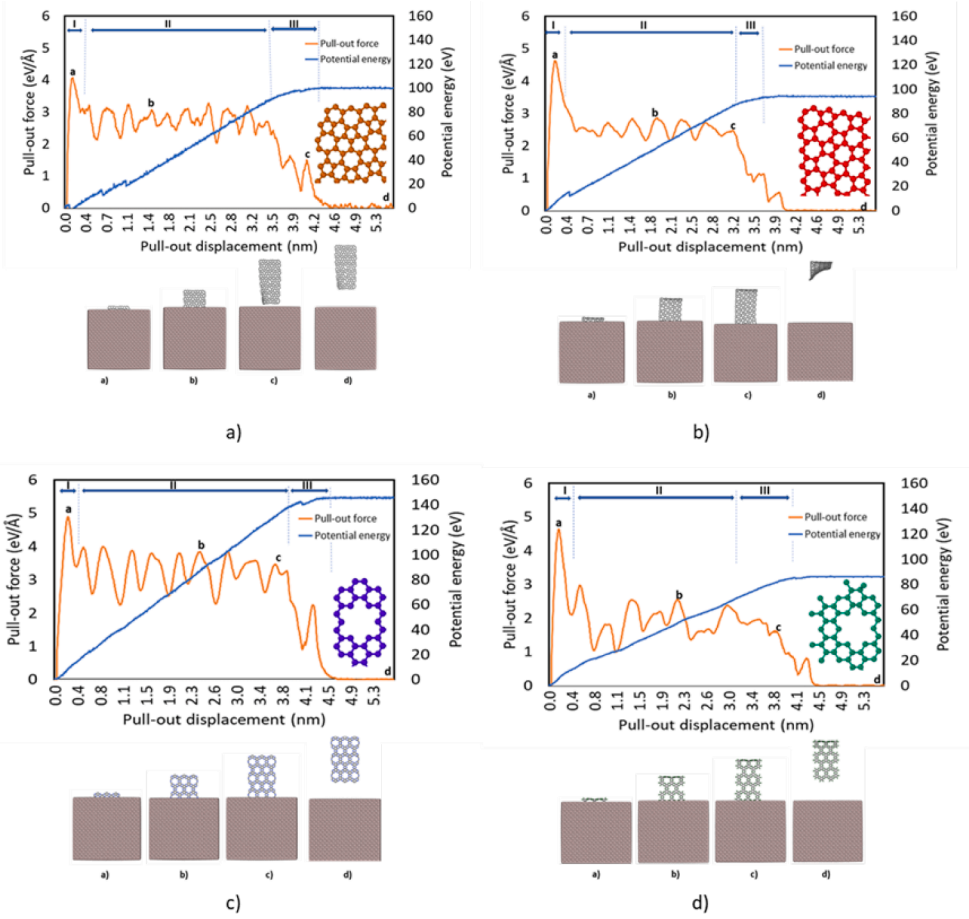

Fig. 3. Pull-out force and potential energy variation as a function of pull-out displacement for **a)** Al-phagraphene; **b)** Al-haeckelite; **c)** Al-N-hG; **d)** Al-B-hG nanocomposites (case A). The snapshots show the atomic configurations at different pull-out displacements.

Table 5
Data on the maximum pull-out force F_{max} (measured in stage I), overall average pull-out force F^{av} (calculated in stages I + II + III), and stationary phase average pull-out force F_{sav} (calculated in stage II), and corresponding interfacial shear strength τ (**case A**).

Structure	F_{max} (eV/Å)	τ_{max} (MPa)	F_{av} (eV/Å)	τ_{av} (MPa)	F_{sav} (eV/Å)	τ_{sav} (MPa)
Al-graphene	5.0	510	2.0	205	3.2	326
Al-phagraphene	4.1	374	1.9	177	2.8	251
Al-haeckelite	4.6	410	1.6	147	2.5	225
Al-N-hG	4.9	411	2.4	202	3.2	273
Al-B-hG	4.6	349	1.4	110	1.9	144

of 4–5 eV/Å, depending on the graphene configuration. In stage II, the pull-out force is higher for the Al-N-hG nanocomposite (3.2 eV/Å) and lower for the Al-B-hG nanocomposite (1.9 eV/Å). Thus, the interfacial strength is slightly improved when N-hG nanofillers are used in the Al nanocomposite. Finally, the pull-out force drops and tends gradually to zero. The potential energy (blue line in Fig. 3(a)-(d)) increases gradually as the nanofiller is being pull-out from the Al matrix and reaches a maximum value: this value is higher for the Al-N-hG nanocomposite (146 eV) and lower for the Al-B-hG nanocomposite (86 eV).

The pull-out force is closely related to the interfacial strength. The interfacial shear strength is given by [33 34]:

$$\tau = \frac{F}{2A} = \frac{F}{2wL} \tag{3}$$

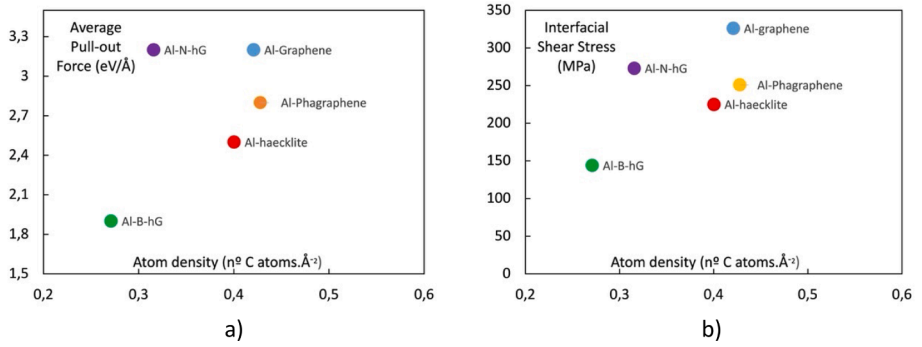

Fig. 4. a) Average pull-out force and b) Interfacial hear strength (τ_{sav}) as function of density of carbon atoms in sheets, during the complete pull-out process (case A).

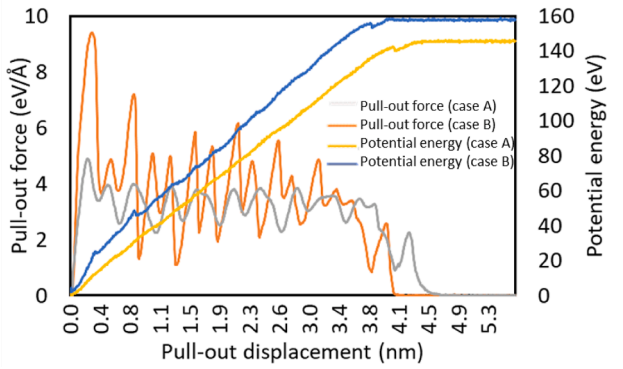

Fig. 5. Variation of pull-out force and potential energy with the pull-out displacement for Al-N-hG nanocomposite before (case A) and after recrystallization (case B). For case A, the pull-out force is represented by the grey curve and the potential energy by the yellow curve. For case B, the pull-out force is represented by the orange curve and the potential energy by the blue curve. (For interpretation of the references to colour in this figure legend, the reader is referred to the web version of this article.)

where w and L are the width and length (in-plane dimensions) of the nanofiller, respectively; and F is the pull-out force. Table 5 presents three relevant values of pull-out force F: (i) the maximum force F_{max} (measured in stage I), (ii) the overall average force F_{av} (calculated in stages I + II + III), and (iii) the stationary phase average force F_{sav} (calculated in stage II). Moreover, the corresponding values of interfacial shear strength τ are also given in Table 5. Due to the stable fluctuation of force in stage II (stationary phase), some authors [15 36] select the average force at stage II to calculate the interfacial shear strength. In order to compare the obtained results with existing ones, only the results obtained in stage II (F_{sav} and τ_{sav}) will be taken into account throughout the discussion.

The pull-out force for Al-graphene obtained here is comparable with existing MD results (between 296 and 351 MPa [15]). The Al-graphene nanocomposite exhibits the highest τ_{sav} values while the Al-B-hG nanocomposite exhibits the lowest τ_{sav} values. Although the interfacial shear strength is usually controlled by the embedded length of nanofiller [15 33] such that it increases in relation to the dimensions of nanofiller, in this investigation, since the length variation between nanofillers is negligible, the influence this parameter has on τ_{sav} is also negligible.

The pull-out force (F_{sav}) and the interfacial shear strength (τ_{sav}), as a function of carbon atom density in the graphene sheets, are presented in Fig. 4. Carbon atom density can be seen as approximately the inverse of porosity in graphene type systems, since less carbon atoms originate more pores, although not necessarily more permeability or bigger pore size.

With the exception on Al-N-hG, the pull-out force and interfacial shear stress between nanofillers and metal matrix show a sharp increase with carbon atom density which means that the existence of pores or hollow regions does not positively influence adhesion between nanofiller and metal matrix, at least when no melting and recrystallization is present. In the case of Al-N-hG (and also Al-B-hG), it can be concluded that the presence of heteroatoms have a determinant influence on the adhesion of these nanocomposites, but this influence can be positive or negative depending on the type of heteroatom.

3.2. Case B – aluminium melted and recrystallized

To facilitate the comparison between case A, where the aluminum matrix is bare, and case B, where the aluminum matrix is previously melted and recrystallized, graph in Fig. 5 is plotted. The Al-N-hG nanocomposite is selected as a representative model. When comparing the results obtained in both cases (A and B), it can be seen that the different pull-out stages are more difficult to discern in case B (orange curve) than in case A (grey curve) due to heavy fluctuations in the pull-out force, probably caused by the grainy recrystallized Al matrix. Similarly to the trend in the potential energy curve of case A (yellow line), the trend in the potential energy curve of case B (blue line) progressively increases as the nanofiller is being pulled-out from the Al matrix. In general, the pull-out force is also higher in case B (orange curve) than in case A (grey curve). Fig. A.1 in the Appendix shows the results obtained in case B for the five nanocomposites with their respective snapshots.

Table 6
Data on the maximum pull-out force F_{max} (measured in stage I), overall average pull-out force F^{av} (calculated in stages I + II + III), and stationary phase average pull-out force F_{sav} (calculated in stage II), and corresponding interfacial shear strength τ (**case B**).

Structure	F_{max} (eV/Å)	τ_{max} (MPa)	F_{av} (eV/Å)	τ_{av} (MPa)	F_{sav} (eV/Å)	τ_{sav} (MPa)
Al-graphene	3.7	378	2.2	220	3.1	315
Al-phagraphene	4.0	364	2.4	215	3.5	321
Al-haeckelite	5.9	526	2.3	209	3.2	288
Al-N-hG	9.4	789	2.8	232	3.9	324
Al-B-hG	5.4	409	2.3	175	3.1	235

Table 7
A comparison of results (interfacial shear strengths τ_{av} and τ_{sav}) between case A (aluminium matrix not modified) and case B (aluminium matrix melted and recrystallized) in terms of percentage.

Structure	$\frac{\tau_{av,B}}{\tau_{av,A}}-1$	$\frac{\tau_{sav,B}}{\tau_{sav,A}}-1$
Al-graphene	+7%	−3%
Al-phagraphene	+21%	+28%
Al-haeckelite	+42%	+28%
Al-N-hG	+15%	+19%
Al-B-hG	+59%	+63%

Table 6 shows the maximum pull-out force F_{max} (measured in stage I), the overall average pull-out force F_{av} (computed in stages I + II + III), and the stationary phase average pull-out force F_{sav} (calculated in stage II), as well as the corresponding values of interfacial shear strength τ. Table 7 shows a comparison between interfacial shear strengths of cases A, where the aluminium matrix was not modified (presented before), and case B, where the aluminium matrix was melted and recrystallized (presented in this section). In case of Al-graphene nanocomposite, the interfacial shear strength is nearly insensitive to the melting and recrystallization of the aluminium matrix. However, melting and recrystallization around a porous holey graphene increases the pull-out force and interfacial shear strength, thus improving the interfacial properties of the nanocomposites. This increase is moderate for Al-phagraphene, Al-haeckelite and Al-N-hG nanocomposites, between 20 and 30%, while it is high for Al-B-hG nanocomposite, about 60%. Fig. 6 shows the variation of average pull-out force and interfacial shear stress with the carbon atom density. It can be observed that the differences between the bare aluminum nanocomposites from Fig. 4 and the melted and recrystalized matrix are substantial, proving that an accurate modelling of the interface of porous nanofillers should be taken into account on the study of the reinforcement of nanocomposites and that there are clear benefits in terms of accuracy by including a simulation step for melting and recrystallization of the metal matrix. This conclusion has also already been recognized by Izadi et al. [37] for polymer nanocomposites, where after building the initial configuration, the nanocomposite is annealed to reach a more stable state.

The increase of pull-out force and interfacial shear stress for the recrystalized metal matrix in comparison to the bare metal matrix should be related to the structural differences in the interface between metal and nanofillers for these two cases. This can be achieved by

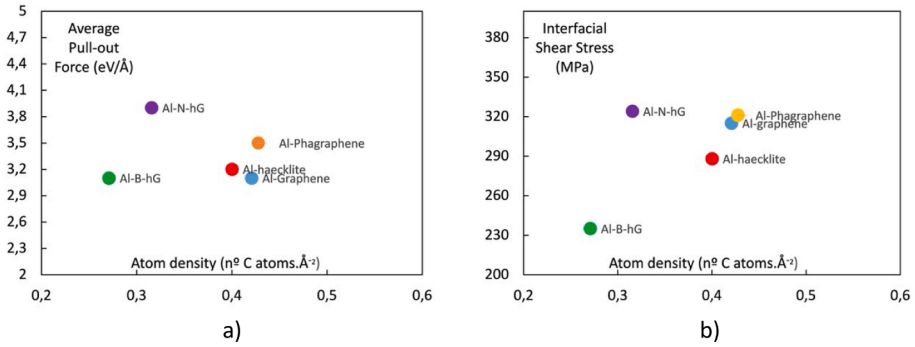

Fig. 6. a) Average pull-out force and b) Interfacial hear strength (τ_{sav}) as function of density of carbon atoms in sheets, during the complete pull-out process (case B).

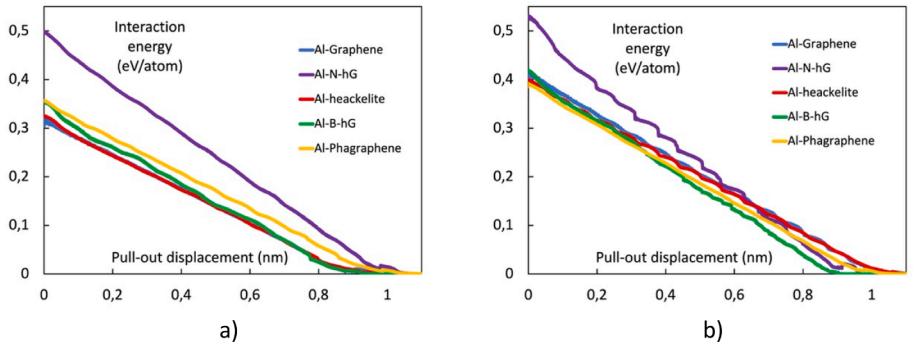

Fig. 7. Variation of interaction energy between nanofiller and metal for a) case A and for b) case B, during the complete pull-out process.

calculating the interaction energy between the two materials in each case. The interaction energy depends on the contact surface between atoms of the nanofillers and metal atoms, that is, the more metal atoms in close proximity to the carbon atoms of the nanofiller the higher the interaction energy. The interaction energy is also function of the proximity between the atoms of the two materials, that is, the closer the atoms, the higher the interaction energy. Fig. 7 a) and b) show the variation of interaction energy the pull-out displacement for the bare matrix case and the recrystalized matrix case, respectively. Before pull-out starts, the interaction energy is maximum for both cases, since the interface is stable and undisturbed, and atoms of both materials are at equilibrated distances. Fig. 6 allows the comparison between the equilibrium interaction energies. Their initial values are clearly higher (Al-graphene + 35%, Al- Phagraphene + 8%, Al-heacklite + 23%, Al-N-hG + 5% and Al-B-hG + 18%) when the metal matrix had been melted and recrystalized. These increases are neither directly related to the existence of pores or hollow vacancies in the nanofillers, nor are they related to the carbon atoms density of the sheets, since the interaction energies are given per atom. These increases in the interaction energy from the bare Al to the recrystalized case may be possibly related to the equilibrated reconstruction of the interface, where the metal atoms have filled all the permitted spaces and are at equilibrium distances from the nanofiller atoms.

As the nanofillers are pulled-out of the metal matrix, the interaction energy linearly drops to zero in both cases. However, unlike the bare metal case, in case B, the interaction energy curves are not rigorously linear but present small cyclic oscillations. These oscillations are related to the porosity of the nanofillers, since the distance between atoms of both materials varies as the nanofiller surface slides out of the metal matrix.

The present work does not address the possible influence of variables such as the nanofillers shape and size, the pulling rate and the temperature on the interfacial adhesion. With respect to the nanofillers size and shape, some work has been done in tubular and planar shapes of graphynes [38] and it was found that the shape of the nanofiller is more determinant than its size. However, given the particular planar defective graphene sheets in our work, a detailed study would have to be conducted to evaluate such effects. The pulling rate should be the lowest possible (in the context of MD) in order to model realistically. The pulling rate used here is in line with the pulling rate used in similar works [39]. Due to the importance of this subject, a detail study of the effects of the pulling rate as well as the temperature will be the focus of future work.

4. Conclusion

This paper presented a computational study on the interfacial mechanical properties of five Al nanocomposites (Al-graphene, Al-phagraphene, Al-haeckelite, Al-N-hG and Al-B-hG). By performing pull-out tests in the context of MD simulations, the potential energy and pull-out force were extracted. Two different matrix cases were dealt in this study: (i) case A, in which the Al matrix was not modified (neither melted nor recrystallized), and (ii) case B, in which the Al matrix was melted and then recrystallized. The following concluding remarks are due:

- The potential energy variations during pull-out processes are clearly higher in recrystallized aluminium matrices than in the bare ones.
- In non-recrystallized aluminium matrices, the pull-out force of Al-N-hG and Al-graphene nanocomposites are similar and higher than the other nanocomposites. However, Al-graphene nanocomposite exhibits the highest interfacial shear strength of all, while Al-B-hG nanocomposite exhibits the lowest pull-out force and interfacial shear strength.
- In recrystallized aluminium matrices, the pull-out force and interfacial shear strength are generally higher, giving rise to improved interfacial properties. The pull-out force and the interfacial shear strength of Al-N-hG nanocomposite are the highest among other nanocomposites. Using the pull-out force per atom of filler for a fair comparison between the nanocomposites, it is clearly seen that the

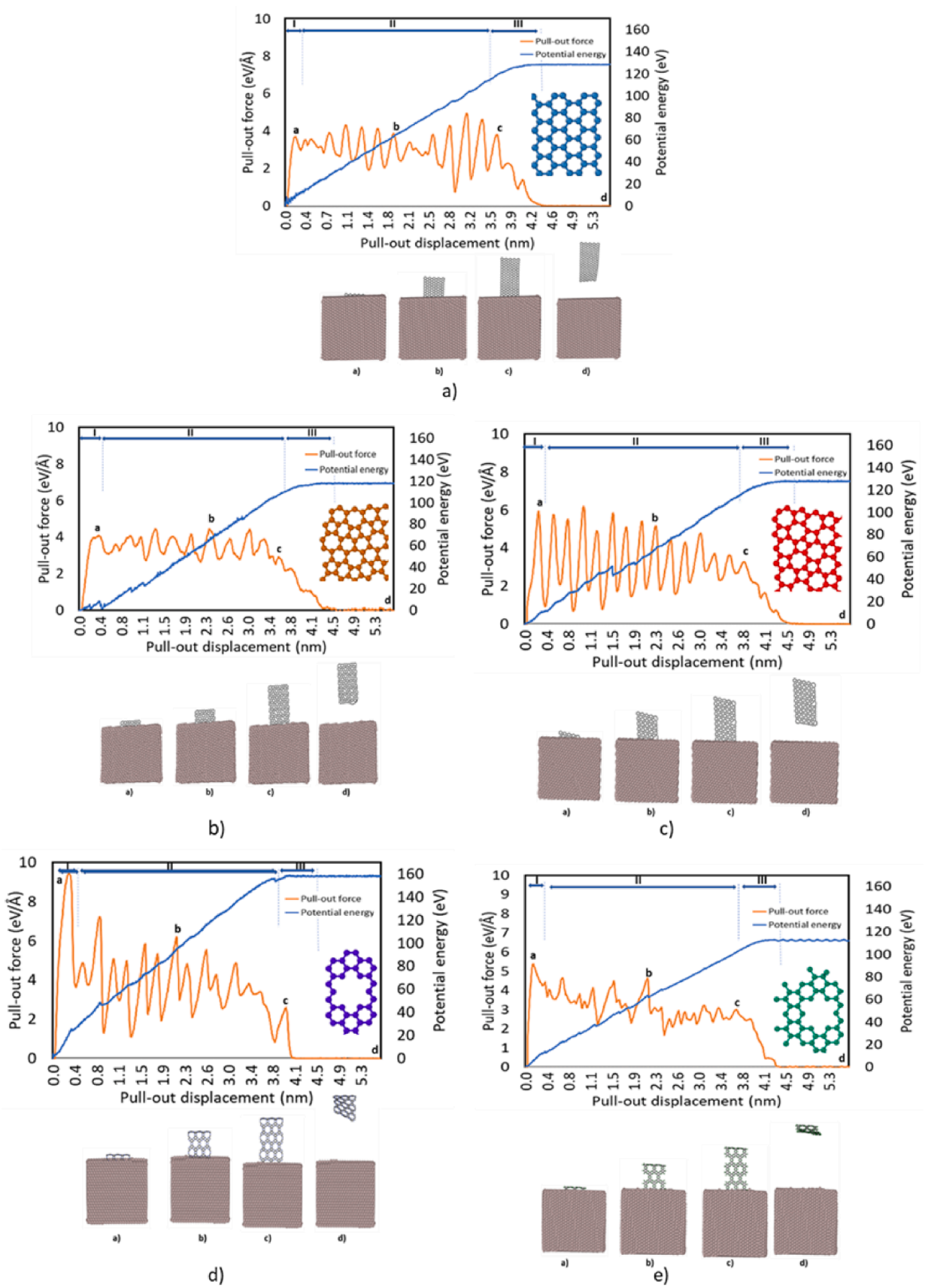

Fig. A1. Pull-out force and potential energy variation as a function of the pull-out displacement for the **a)** Al-graphene; **b)** Al-phagraphene; **c)** Al-haeckelite; **d)** Al-N-hG; **e)** AL-B-hG nanocomposites (case B). The snapshots show the atomic configurations at different pull-out displacements.

presence of holes in graphene (holey graphene) improves the interfacial interaction between graphene and aluminium matrix.

- The increase in pull-out force and interfacial shear strength can be directly related to the interaction energies for both materials at the interface. These interaction energies show the structural differences between the interfaces in both cases. The melted and recrystalized interfaces have higher interaction energies because atoms are closer and have a wider contact surface (more wrinkled), since they occupy all the available space close to the nanofiller at actual equilibrium distances.
- A strong adhesion between nanofiller and Al matrix does not necessarily imply a better reinforcement of the Al matrix, since also the mechanical properties of the nanofiller have to be taken in account.
- The aluminium-based nanocomposites should be modelled using a melted and recrystallized aluminium matrix (case B), because that is the best approach to understand the real effect of the pores of the nanofillers. Its clearly beneficial to use holey-graphenes in aluminium nanocomposites because they improve the interfacial properties, despite their lower intrinsic mechanical properties compared to graphene.

CRediT authorship contribution statement

Cátia Guarda: Data curation, Formal analysis, Investigation, Methodology, Software, Visualization, Writing – original draft. **Bruno Faria:** Conceptualization, Data curation, Formal analysis, Investigation, Methodology, Software, Visualization, Writing – original draft. **Nuno Silvestre:** Conceptualization, Methodology, Funding acquisition, Supervision, Validation, Writing – review & editing. **José N. Canongia Lopes:** Conceptualization, Methodology, Funding acquisition, Supervision, Validation, Writing – review & editing.

Declaration of Competing Interest

The authors declare that they have no known competing financial interests or personal relationships that could have appeared to influence the work reported in this paper.

Data availability

No data was used for the research described in the article.

Acknowledgements

This work was supported by FCT, through IDMEC, under LAETA, project UIDB/50022/2020, through Centro de Química Estrutural (CQE), project UIDB/00100/2020 and through Institute for Polymers and Composites. The first author gratefully acknowledges the financial support given by FCT in the context of the PhD scholarship SFRH/BD/129589/2017. The second author gratefully acknowledges the financial support given by FCT in the context of the Postdoctoral contract CEECINST/00156/2018.

Appendix A

References

[1] Ovid'ko I. Metal-graphene nanocomposites with enhanced mechanical properties: a review, Metal-graphene nanocomposites with enhanced mechanical properties: a review, vol. 38, 2014, pp. 190-200.
[2] Duan K, et al. Interface mechanical properties of graphene reinforced copper nanocomposites. Mater Res Express 2017;4:115020.
[3] Wang J, et al. Reinforcement with graphene nanosheets in aluminum matrix composites. Scr Mater 2012;66:594–7.
[4] Dixit S, et al. Multi-layer graphene reinforced aluminum—manufacturing of high strength composite by friction stir alloying. Composites B 2018;136:63–71.
[5] Shin S, et al. Strengthening behavior of few-layered graphene/aluminum composites. Carbon 2015;82:143–51.
[6] Rashad M, et al. Investigation on microstructural, mechanical and electrochemical properties of aluminum composites reinforced with graphene nanoplatelets. Prog Nat Sci: Mater Int 2015;25:460–70.
[7] Zhu J, Yang Q, Liu X. Investigation on the Tensile Behavior of Graphene-Aluminum Nano-Laminated Composites by Molecular Dynamics Simulation. Eng Mater 2019;804:1–6.
[8] Mokhalingam A, Kumar D, Srivastava A. Mechanical Behaviour of Graphene Reinforced Aluminum Nanocomposites. Mater Today: Proc 2017;4:3952–8.
[9] Liu J, et al. Mechanical properties of graphene-reinforced aluminium composite with modified substrate surface: a molecular dynamics study. Nanotechnology 2021;32:085712.
[10] Montazeri A, Panahi B. MD-based estimates of enhanced load transfer in graphene/metal nanocomposites through Ni coating. Appl Surf Sci 2018;457:1072–80.
[11] Wang X, et al. Enhanced interfacial strength of graphene reinforced aluminum composites via X (Cu, Ni, Ti)-coating: Molecular-dynamics insights. Adv Powder Technol 2021;32:2585–90.
[12] Hopkins PE, et al. Manipulating Thermal Conductance at Metal-Graphene Contacts via Chemical Functionalization. Nano Lett 2012;12:590–5.
[13] Zhang X, Wang S. Interfacial Strengthening of Graphene/Aluminum Composites through Point Defects: A First-Principles Study. Nanomaterials 2021;11:738.
[14] Zhou X, et al. Atomic simulations of the formation of twist grain boundary and mechanical properties of graphene/aluminum nanolaminated composites. Comput Mater Sci 2020;172:109342.
[15] Zhu J, et al. Micro-Mechanism of Interfacial Separation and Slippage of Graphene/Aluminum Nanolaminated Composites. Nanomaterials 2018;8:1046.
[16] Guarda C, et al. Melted and recrystallized holey-graphene-reinforced aluminum composites: Structure, elasticity and strength. Compos Struct 2022;292:115679.
[17] Humphrey W, Dalke A, Schulten K. VMD: Visual molecular dynamics. J Mol Graphics 1996;14(1):33–8.
[18] "VMD - Visual Molecular Dynamics," 1996. [Online]. Available: https://www.ks.uiuc.edu/Research/vmd/. [Accessed 18 January 2022].
[19] Hanwell MD, et al. Avogadro: An advanced semantic chemical editor, visualization, and analysis platform. Journal of Cheminformaitcs 2012;4(1):17.
[20] "VESTA - Visualization for Electronic and Structural Analysis," 2005. [Online]. Available: http://jp-minerals.org/vesta/en/. [Accessed 18 January 2022].
[21] Plimpton S. Fast Parallel Algorithms for Short-Range Molecular Dynamics. J Comput Phys 1995;117:1–19.
[22] Stukowski A. Visualization and analysis of atomistic simulation data with OVITO-the Open Visualization Tool. Model Simul Mater Sci Eng 2010;18:015012.
[23] Tersoff J. Modeling solid-state chemistry: Interatomic potentials for multicomponent systems. Phys Rev B 1989;39:5566.
[24] Kinaci A, et al. Thermal conductivity of BN-C nanostructures. Phys Rev B 2012;86:115410.
[25] Mendelev MI, et al. Analysis of semi-empirical interatomic potentials appropriate for simulation of crystalline and liquid Al and Cu. Phil Mag 2008;88:1723–50.
[26] Boda D, Henderson D. The effects of deviations from Lorentz-Berthelot rules on the properties of a simple mixture. Mol Phys: Int J Interface Between Chem Phys 2008;106:2367–70.
[27] Kutana A, Giapis KP. Transient deformation regime in bending of single-walled carbon nanotubes. Phys Rev Lett 2006;97:245501.
[28] Vekeman J, et al.. Nitrogen Gas on Graphene: Pairwise Interaction Potentials. Int Conf Computational Sci Appl 2018;10964:563–78.
[29] Fan L, Yao W. Mechanical properties of a G/h-BN heterobilayer nanosheets coupled by interlayer sp3 defects. Mater Res Express 2019;6:095075.
[30] Munilla J, Castro M, Carnicero A. Surface effects in atomistic mechanical simulations of Al nanocrystals. Phys Rev B 2009;80:024109.
[31] Wang Z, et al. Phagraphene: A Low-Energy Graphene Allotrope Composed of 5–6–7 Carbon Rings with Distorted Dirac Cones. Nano Letter 2015;15:6182–6.
[32] Lin Y, et al. Holey graphene: a unique structural derivative of graphene. Mater Res Lett 2017;5:209–34.
[33] Zhao S, et al. Significantly improved interfacial shear strength in graphene/copper nanocomposite via wrinkles and functionalization: A molecular dynamics study. Carbon 2021;174:335–44.
[34] Zhang X, et al. A powder-metallurgy-based strategy toward three-dimensional graphene-like network for reinforcing copper matrix composites. Nat Commun 2020;11:2775.
[35] Mohammad UHJ, et al. Porosity. Springer Cham; 2016.
[36] Lv C, et al. Effect of Chemisorption on the Interfacial Bonding Characteristics of Graphene-Polymer Composites. J Phys Chem C 2010;114:6588–94.
[37] Izadi R, Ghavanloo E, Nayebi A. Elastic properties of polymer composites reinforced with C60 fullerene and carbon onion: Molecular dynamics simulation. Phys B Condens Matter 2019;574:311636.
[38] Faria B, Guarda C, Silvestre N, Lopes JNC. Aluminum composites reinforced by γ-graphynes: The effect of nanofillers porosity and shape on crystal growth and composite strengthening. Comput Mater Sci Apr. 2020;176:109538.
[39] Wang X, et al. Enhanced interfacial strength of graphene reinforced aluminum composites via X (Cu, Ni, Ti)-coating: Molecular-dynamics insights. Adv Powder Technol Jul. 2021;32(7):2585–90.